Frontiers of Information Technology & Electronic Engineering
www.zju.edu.cn/jzus; engineering.cae.cn; www.springerlink.com
ISSN 2095-9184 (print); ISSN 2095-9230 (online)
E-mail: jzus@zju.edu.cn

A modified variable rate particle filter for maneuvering target tracking*

Yun-fei GUO†, Kong-shuai FAN, Dong-liang PENG, Ji-an LUO, Han SHENTU
(*Automation School, Hangzhou Dianzi University, Hangzhou 310018, China*)
†E-mail: gyf@hdu.edu.cn

Received May 6, 2015; Revision accepted June 23, 2015; Crosschecked Oct. 20, 2015

Abstract: To address the problem of maneuvering target tracking, where the target trajectory has prolonged smooth regions and abrupt maneuvering regions, a modified variable rate particle filter (MVRPF) is proposed. First, a Cartesian-coordinate based variable rate model is presented. Compared with conventional variable rate models, the proposed model does not need any prior knowledge of target mass or external forces. Consequently, it is more convenient in practical tracking applications. Second, a maneuvering detection strategy is adopted to adaptively adjust the parameters in MVRPF, which helps allocate more state points at high maneuver regions and fewer at smooth regions. Third, in the presence of small measurement errors, the unscented particle filter, which is embedded in MVRPF, can move more particles into regions of high likelihood and hence can improve the tracking performance. Simulation results illustrate the effectiveness of the proposed method.

Key words: Maneuvering target tracking, Prolonged smooth regions, Variable rate model, Maneuver detection
doi:10.1631/FITEE.1500149 **Document code:** A **CLC number:** TN953

1 Introduction

Maneuvering target tracking (MTT), as an important issue in the target tracking field, has received considerable interest in recent years (Bar-Shalom and Li, 1995; Bar-Shalom *et al.*, 2001). The major challenge of MTT is the target motion uncertainty (Li and Jilkov, 2003; Yang *et al.*, 2015); in other words, the key to successful tracking of a maneuvering target is choosing an appropriate model for the target's current motion from measurements (Schoenecker *et al.*, 2013; Nemeth *et al.*, 2014). The existing various modeling methods may be divided into two main categories: the single-model method and the multi-model method (Li and Jilkov, 2010). The former manages to design a suitable model whose structure or parameters can be adjusted adaptively in the case that the target maneuvers. The single-model method has the advantage of simplicity and lower computational complexity. However, it cannot match the target's maneuvering behavior immediately due to the delay in maneuver detection (Ru *et al.*, 2009; Zhang and Geng, 2013). The latter model assumes that the target motion can be described by one of multiple models or by a suitable combination of them. The multi-model method can automatically match the target maneuvering behavior by updating each model's weight. In addition, it can obtain a more accurate state estimate at the cost of higher computational complexity (Li and Jilkov, 2010).

All the above methods are fixed rate methods, in which the state variable is assumed to evolve synchronously with the observation time and the state is updated upon a new arrival measurement. In practice, however, the target often makes a prolonged non-maneuvering motion, with abrupt, but

* Project supported by the National Natural Science Foundation of China (No. 61174024)
ORCID: Yun-fei GUO, http://orcid.org/0000-0001-7887-4312

infrequent, maneuvering behaviors (Schoenecker *et al.*, 2013; Nemeth *et al.*, 2014). To characterize the target trajectory in a more natural and realistic manner, a variable rate method has been proposed by Godsill *et al.* (2007) and Whiteley *et al.* (2011). In this method, the state arriving time is assumed to be a random variable with known distribution and to propagate asynchronously with the observation time. It leads to an associated reduction in computational complexity and storage requirement (Bunch and Godsill, 2013), especially in the high scan rate case. However, there are some problems in the original variable rate method. First, previous variable rate models are based on intrinsic coordinates, where prior knowledge about target mass, external normal force, and external tangential force is needed (Godsill *et al.*, 2007; Ulker and Gunsel, 2012). In the case of tracking noncooperative targets, it is difficult to obtain these parameters. In addition, most existing radar or sonar systems are based on Cartesian or polar coordinates (Bar-Shalom and Li, 1995), and the intrinsic coordinate based method cannot be directly applied in these systems. Second, the distribution of state sojourn time in the original variable rate method is time-invariant during the observation period. Consequently, the original variable rate method cannot allocate automatically more state points at high maneuver regions due to its inability of detecting maneuvering. To address the second problem, a multi-model based variable rate method has been presented by Ulker and Gunsel (2012). The tracking performance is improved at the cost of higher computational complexity and more storage.

To address these two aforementioned problems, a modified variable rate particle filter (MVRPF) is proposed. It has three major contributions. First, a variable rate model in Cartesian coordinates is derived. Compared with that in the intrinsic coordinates, it does not need prior information on target mass or external forces. In addition, it is more convenient for implementation and incorporation with existing tracking methods and systems. Second, to optimize the state point distribution, without additional computational or storage requirement, a maneuver-detection strategy is adopted in MVRPF. The parameters of the model will be adjusted once the target maneuver is detected. Third, an unscented particle filter is embedded in MVRPF to establish the proposal density function, which leads to more particles locating in high likelihood regions and hence improves the estimation performance in the presence of small measurement errors.

2 Variable rate model in Cartesian coordinates

Previous variable rate methods usually model the target state in intrinsic coordinates, where the target motion is subject to both a tangential acceleration and a normal acceleration (Godsill *et al.*, 2007; Bunch and Godsill, 2013). Although the intrinsic-coordinate model is more realistic compared with conventional models, such as the Cartesian- or polar-coordinate model, there are two drawbacks which hinder its wide application. First, to describe the target dynamic motion, more prior knowledge is needed, such as knowledge about target mass, tangential force, and normal force (Godsill *et al.*, 2007). However, it is usually difficult to obtain these parameters for a noncooperative target (Bar-Shalom *et al.*, 2001; Li and Jilkov, 2003). Second, it is more complex in model representation, implementation, and calculation. To address these problems, a modified Cartesian-coordinate based variable rate model is presented in this section. In this method, some prior knowledge about the target, such as target mass and external force, is unnecessary. This modification makes the variable rate model more convenient, and helps incorporate it into many existing tracking techniques and systems which are carried out in Cartesian coordinates.

In a variable rate model framework, the underlying state process is assumed to be asynchronous with the measurement process (Ulker and Gunsel, 2012), which means that the state arriving time is not the same as the measurement time. A general Markovian model in terms of the condition probability density function (pdf) is adopted to describe the state evolving process:

$$\boldsymbol{X}_t \sim p(\boldsymbol{X}_t|\boldsymbol{X}_{t-1}), \tag{1}$$

where t is a discrete state time index and the state variable $\boldsymbol{X}_t$ is composed of a state arrival time τ_t and a sub-state vector $\boldsymbol{\theta}_t$, i.e., $\boldsymbol{X}_t = [\tau_t, \boldsymbol{\theta}_t]^{\mathrm{T}}$. The state arrival time (τ_t) is assumed to be monotonically increasing, $\tau_t > \tau_{t-1}$, and satisfies the following shifted

gamma distribution (Godsill *et al.*, 2007):

$$\tau_t \sim p(\tau_t|\tau_{t-1}) = \tau_{t-1} + \tau_{\min,t} + G(\alpha_t, \beta_t), t = 1, 2, ..., T, \quad (2)$$

where $\tau_{\min,t}$, α_t, and β_t are three designed nonnegative parameters of the gamma distribution and T is the maximum state arrival time index. The sub-state vector $\boldsymbol{\theta}_t \triangleq [\boldsymbol{\eta}_t, \boldsymbol{a}_t]^{\mathrm{T}}$ is characterized by a Markovian model as follows:

$$\boldsymbol{\theta}_t \sim p(\boldsymbol{\theta}_t|\boldsymbol{\theta}_{t-1}, \tau_{t-1}), \quad (3)$$

where $\boldsymbol{\eta}_t \triangleq [\boldsymbol{\xi}(\tau_t), \dot{\boldsymbol{\xi}}(\tau_t)]^{\mathrm{T}}$ is named the kinematic component in this study, which is composed of a position vector $\boldsymbol{\xi}(\tau_t)$ and a velocity vector $\dot{\boldsymbol{\xi}}(\tau_t)$. Also, $\boldsymbol{a}_t$ defined in the Cartesian coordinates is an acceleration vector or process noise, which drives the target's motion. If no prior knowledge is available, the acceleration is assumed to follow a Gaussian distribution, i.e., $\boldsymbol{a}_t \sim N(0, \boldsymbol{Q}_t)$, where $\boldsymbol{Q}_t$ is a designed parameter. Then the kinematic vector can be calculated as follows:

$$\dot{\boldsymbol{\xi}}(\tau_t) = \dot{\boldsymbol{\xi}}(\tau_{t-1}) + \delta_t \boldsymbol{a}_{t-1}, \quad (4)$$

$$\boldsymbol{\xi}(\tau_t) = \boldsymbol{\xi}(\tau_{t-1}) + \delta_t \dot{\boldsymbol{\xi}}(\tau_{t-1}) + 0.5\delta_t^2 \boldsymbol{a}_{t-1}, \quad (5)$$

where $\delta_t \triangleq \tau_t - \tau_{t-1}$ is the state sojourn time between τ_{t-1} and τ_t. Compared with the intrinsic-coordinate based model which needs complicated integral operations to calculate the kinematic vector (Godsill *et al.*, 2007; Bunch and Godsill, 2013), the Cartesian-coordinate based model is much simpler. Then one has

$$p(\boldsymbol{X}_t|\boldsymbol{X}_{t-1}) = p(\boldsymbol{\theta}_t|\boldsymbol{\theta}_{t-1}, \tau_{t-1}) p(\tau_t|\tau_{t-1}). \quad (6)$$

Since the rate of measurements is generally different from that of the state process (Whiteley *et al.*, 2011), a neighborhood of states must be defined before characterizing the observation model. In a variable rate model framework, a measurement $\boldsymbol{z}_k$ at measurement time k is assumed to be conditional only upon a neighborhood of $\boldsymbol{X}_{\boldsymbol{\mathcal{N}}_k} = \{\boldsymbol{X}_t : t \in \boldsymbol{\mathcal{N}}_k(x_{0:\infty})\}$. The neighborhood $\boldsymbol{\mathcal{N}}_k$ contains the state time index whose corresponding arrival times are closest to the measurement time k. For simplicity, it is assumed that there are only two components contained in the neighborhood in this study, $\boldsymbol{\mathcal{N}}_k = [\mathcal{N}_k^-, \mathcal{N}_k^+]$, where $\mathcal{N}_k^- = \min(\boldsymbol{\mathcal{N}}_k)$, $\mathcal{N}_k^+ = \max(\boldsymbol{\mathcal{N}}_k)$, and $\mathcal{N}_k^- \geq \mathcal{N}_{k-1}^-$, $\mathcal{N}_k^+ \geq \mathcal{N}_{k-1}^+$ (Godsill *et al.*, 2007). Then a general observation model at time k can be given as follows:

$$\boldsymbol{z}_k \sim p(\boldsymbol{z}_k|\boldsymbol{X}_{\boldsymbol{\mathcal{N}}_k}) = p(\boldsymbol{z}_k|\hat{\boldsymbol{\eta}}_k), \quad (7)$$

where $\hat{\boldsymbol{\eta}}_k \triangleq \hat{\boldsymbol{\eta}}_k(\boldsymbol{X}_{\boldsymbol{\mathcal{N}}_k})$ is a deterministic interpolation function and is dependent on the state neighborhood. For simplicity, a linear interpolation function may be used, that is,

$$\hat{\boldsymbol{\eta}}_k = \frac{(k - \tau_{\mathcal{N}_k^-})\boldsymbol{\eta}_{\mathcal{N}_k^+} + (\tau_{\mathcal{N}_k^+} - k)\boldsymbol{\eta}_{\mathcal{N}_k^-}}{\mathcal{N}_k^+ - \mathcal{N}_k^-}. \quad (8)$$

From a Bayesian perspective, the tracking problem with a variable rate model is to estimate recursively the state up to the end of the current neighborhood $\boldsymbol{\mathcal{N}}_k$, i.e., $t = \mathcal{N}_k^+$, given the measurement sequence $\boldsymbol{z}_{0:k}$. Assume that the initial prior pdf $p(\boldsymbol{X}_{\mathcal{N}_0^+})$ is available. Then the posterior pdf $p(\boldsymbol{X}_{\mathcal{N}_k^+}|\boldsymbol{z}_{0:k})$ can be obtained recursively in two stages: prediction and update. Suppose that the posterior pdf at time $k-1$ is $p(\boldsymbol{X}_{\mathcal{N}_{k-1}^+}|\boldsymbol{z}_{0:k-1})$. The predictive pdf can be obtained via the following Chapman-Kolmogorov equation:

$$p(\boldsymbol{X}_{\mathcal{N}_k^+}|\boldsymbol{z}_{0:k-1}) = \int p(\boldsymbol{X}_{\mathcal{N}_k^+}|\boldsymbol{X}_{\mathcal{N}_{k-1}^+}) \cdot p(\boldsymbol{X}_{\mathcal{N}_{k-1}^+}|\boldsymbol{z}_{0:k-1}) \mathrm{d}\boldsymbol{X}_{\mathcal{N}_{k-1}^+}. \quad (9)$$

At time k, the new arrival measurement $\boldsymbol{z}_k$ can be used to calculate the posterior pdf via the Bayes rule:

$$p(\boldsymbol{X}_{\mathcal{N}_k^+}|\boldsymbol{z}_{0:k}) = \frac{p(\boldsymbol{z}_k|\boldsymbol{X}_{\mathcal{N}_k^+}) p(\boldsymbol{X}_{\mathcal{N}_k^+}|\boldsymbol{z}_{0:k-1})}{p(\boldsymbol{z}_k|\boldsymbol{z}_{0:k-1})}, \quad (10)$$

where

$$p(\boldsymbol{z}_k|\boldsymbol{z}_{0:k-1}) = \int p(\boldsymbol{z}_k|\boldsymbol{X}_{\mathcal{N}_k^+}) p(\boldsymbol{X}_{\mathcal{N}_k^+}|\boldsymbol{z}_{0:k-1}) \mathrm{d}\boldsymbol{X}_{\mathcal{N}_k^+}$$

is the normalizing constant. Thus, the variable rate model in Cartesian coordinates has been established and the posterior pdf is given in a Bayesian framework. It is shown that the proposed variable rate model does not need prior knowledge of target mass or external force, and hence it is more suitable for tracking noncooperative targets. In addition, compared with the intrinsic-coordinate based variable rate model, the proposed model is much simpler and more convenient.

3 MVRPF algorithm

Although the original variable rate particle filter (VRPF) method can represent a target trajectory

with fewer state points (Godsill *et al.*, 2007), it cannot automatically allocate more state points in the high maneuver regions and fewer in the smooth regions (Ulker and Gunsel, 2012). In other words, the distribution of state points, which relies on the distribution of state sojourn time, is random and uncontrollable. However, to achieve satisfactory performance, more state points are expected when a maneuver occurs and fewer state points are needed during constant-velocity motion periods. In Ulker and Gunsel (2012), a multi-model VRPF has been presented to optimize the distribution of state points, at the cost of more computational time and storage. In this section, a modified single-model VRPF method is proposed, which can adaptively adjust the parameters with a maneuver-detection strategy. Compared with previous methods, the proposed method improves the tracking performance in a computationally efficient manner. Fig. 1 illustrates the block diagram of MVRPF. For a general nonlinear filter problem, it is not possible to obtain an optimal solution in most cases (Zhang *et al.*, 2015). Here, the particle filter is chosen to provide a suboptimal numerical solution with the variable rate model in Cartesian coordinates. N weighted particles are used to approximate the following posterior pdf:

$$p(\boldsymbol{X}_{\mathcal{N}_k^+}|\boldsymbol{z}_{0:k}) \approx \sum_{i=1}^{N} w_k^i \delta(\boldsymbol{X}^i_{\mathcal{N}_k^+} - \boldsymbol{X}_{\mathcal{N}_k^+}), \tag{11}$$

where $\delta(\cdot)$ is the Dirac-Delta function, and $\boldsymbol{X}^i_{\mathcal{N}_k^+}$, w_k^i are the ith particle and associated weight, respectively. In general, it is not easy to directly draw particles from the true posterior pdf. An important proposal pdf denoted by $q(\cdot)$, whose distribution is known and easy to sample, is used to generate particles. Thus, the weight can be calculated as follows:

$$w_k^i \propto w_{k-1}^i \frac{p(\boldsymbol{z}_k|\boldsymbol{X}^i_{\mathcal{N}_k^+}) p(\boldsymbol{X}^i_{\mathcal{N}_k^+}|\boldsymbol{X}^i_{\mathcal{N}_{k-1}^+})}{q(\boldsymbol{X}^i_{\mathcal{N}_k^+}|\boldsymbol{X}^i_{\mathcal{N}_{k-1}^+}, \boldsymbol{z}_{0:k})}. \tag{12}$$

The most popular and simplest choice of the proposal pdf is the state transition prior model. Although this choice is easier to implement, it does not incorporate the latest arrival measurement $\boldsymbol{z}_k$. When the measurement error is small, the corresponding likelihood is sharp enough and there is little overlap between the likelihood and proposal pdf. In this case, choosing the state prior model as the proposal pdf leads to fewer particles falling into regions of high likelihood, and hence the performance degrades (van der Merwe *et al.*, 2000). In fact, there are many better choices for the proposal pdf as long as its support covers the posterior pdf (Zuo *et al.*, 2013). Although the unscented particle filter (UPF) (van der Merwe *et al.*, 2000) is adopted to establish the proposal pdf in this study, other versions of PF can also work.

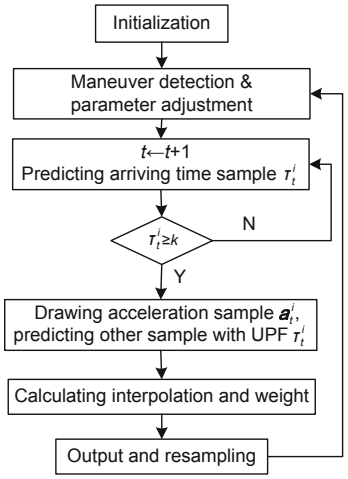

Fig. 1 The MVRPF block diagram

3.1 Initialization

At initial measurement time, $k = 0$, draw N particles $\{\boldsymbol{X}^i_{t(i)}\}_{i=1}^N$ from the prior $p(\boldsymbol{X}_0)$ with equal weights $w_0^i = 1/N$, $i = 1, 2, \ldots, N$, where $t(i)$ is the initial state time index and is set to zero, i.e., $t(i) = 0$. For brevity, the state time index subscript $t(i)$ is simplified as t in the following. For each particle, let its initial state arriving time and initial neighborhood be zero, i.e., $\tau_0^i = 0$, $\boldsymbol{\mathcal{N}}_0^i = [\mathcal{N}_0^{i,-}, \mathcal{N}_0^{i,+}] = [0, 0], i = 1, 2, \ldots, N$. Calculate the mean and the covariance of each particle's kinematic component as follows (van der Merwe *et al.*, 2000):

$$\bar{\boldsymbol{\eta}}_0^i = E[\boldsymbol{\eta}_0^i], \tag{13}$$

$$\boldsymbol{P}_0^i = E[(\boldsymbol{\eta}_0^i - \bar{\boldsymbol{\eta}}_0^i)(\boldsymbol{\eta}_0^i - \bar{\boldsymbol{\eta}}_0^i)^{\mathrm{T}}]. \tag{14}$$

Since all particles have the same weight at the initial stage, the initial output can be evaluated as $\bar{\boldsymbol{\eta}}_0 = \bar{\boldsymbol{\eta}}_0^i$ and $\boldsymbol{P}_0 = \boldsymbol{P}_0^i$. Then calculate the initial measurement prediction $\hat{\boldsymbol{z}}_{1|0}$ and its covariance $\boldsymbol{S}_{1|0}$ with $\bar{\boldsymbol{\eta}}_0$ and $\boldsymbol{P}_0$ using a nonlinear filter, such as the unscented Kalman filter (UKF) (Julier *et al.*, 2000).

3.2 Maneuver detection and parameter adjustment

To improve the tracking performance during the whole surveillance period, a maneuver-detection technique is used to adaptively adjust parameters in MVRPF. The parameters can be classified into two types according to their effects on the algorithm. The first one is the process noise level parameter, i.e., $\boldsymbol{Q}_t$, which characterizes the uncertainty or reliability of the model and affects the estimation accuracy. The second one is the shifted gamma distribution parameters, i.e., $\tau_{\min,t}$, α_t, and β_t (Eq. (2)), which describe the distribution of the state sojourn time and affect the number of state points allocated during a given period. More detailed adjustment strategies of these parameters are analyzed as follows:

1. Process noise level parameter ($\boldsymbol{Q}_t$)

For a single-model MTT algorithm, the choice of the process noise parameter is a trade-off between the estimation performance during maneuvering periods and that during non-maneuvering periods (Bar-Shalom *et al.*, 2001). A high process noise level $\boldsymbol{Q}_t$ increases model uncertainty and helps cover the target's maneuvering behaviors. However, it leads to performance degradation during non-maneuvering periods. Conversely, a low process noise level $\boldsymbol{Q}_t$ leads to better accuracy in smooth regions and worse performance in maneuvering regions. Consequently, a good strategy for adjusting process noise level parameter is increasing $\boldsymbol{Q}_t$ during maneuvering periods and reducing $\boldsymbol{Q}_t$ during non-maneuvering periods.

2. Shifted gamma distribution parameters ($\tau_{\min,t}$, α_t, and β_t)

In the conventional fixed rate method, the state sojourn time (δ_t) is usually assumed to be fixed and is equal to the sensor sampling time. However, in the variable rate method, the state sojourn time (δ_t) is random and depends on the sum of $\tau_{\min,t}$ and $G(\alpha_t,\beta_t)$. For a given observation period, the smaller the state sojourn time is, the more state points are allocated. Since the expectation of gamma distribution equals the product of shape parameter α_t and scale parameter β_t, the expectation of state sojourn time can be calculated as $E(\delta_t)=\tau_{\min,t}+\alpha_t\beta_t$. Thus, a proper strategy for adjusting shifted gamma distribution parameters is increasing $E(\delta_t)$ during non-maneuvering periods and reducing $E(\delta_t)$ during maneuvering periods.

From the above analyses, the generic qualitative relationship between the parameters and tracking performance is given. The quantitative relationship between them is difficult to obtain at this stage. In many tracking applications, such as passive coherent location, the choice of parameters depends on not only the algorithm but also the tracking geometry.

There are many maneuver-detection methods. A comprehensive summary has been presented by Ru *et al.* (2009). For simplicity, a measurement residual based Chi-square test technique is used in this study, although more complex and reliable detection approaches are available (Ru *et al.*, 2009; Nemeth *et al.*, 2014). It is not the main concern of this study to propose a new maneuver-detection method. Assume that the measurement prediction and its covariance at measurement time $k-1$ are denoted by $\hat{\boldsymbol{z}}_{k|k-1}$ and $\boldsymbol{S}_{k|k-1}$, respectively. Then one can obtain the measurement residual $\tilde{\boldsymbol{z}}_k=\boldsymbol{z}_k-\hat{\boldsymbol{z}}_{k|k-1}$ upon the new arrival measurement $\boldsymbol{z}_k$. Under the hypothesis that the target does not maneuver at time k, the measurement residual should be zero mean, Gaussian, and white: $\tilde{\boldsymbol{z}}_k\sim N(0,\boldsymbol{S}_{k|k-1})$. Then one can claim that the target maneuvers at time k if the following Chi-square test holds (Ru *et al.*, 2009):

$$\epsilon_k^l\triangleq\sum_{j=k-l+1}^{k}\epsilon_k=\sum_{j=k-l+1}^{k}\tilde{\boldsymbol{z}}_k^{\mathrm{T}}\boldsymbol{S}_{k|k-1}^{-1}\tilde{\boldsymbol{z}}_k>\chi^2_{ln_z}(\kappa),\tag{15}$$

where l is the sliding window width, n_z the dimension of measurement, and $1-\kappa$ the confidence level of the test.

3.3 Prediction and update

Assume that the state posterior pdf at measurement time $k-1$ is denoted by the weighted particles $\{\boldsymbol{X}^i_{\mathcal{N}^{i,+}_{k-1}},w^i_{k-1}\}_{i=1}^N$. The neighborhood and the newest state arriving time of the ith particle are denoted by $\boldsymbol{\mathcal{N}}^i_{k-1}=[\mathcal{N}^{i,-}_{k-1},\mathcal{N}^{i,+}_{k-1}]$ and $t=\mathcal{N}^{i,+}_{k-1}$, respectively. Also, the neighborhood state kinematic component at time $k-1$ is denoted by $\bar{\boldsymbol{\eta}}^i_{\mathcal{N}^{i,+}_{k-1}}$ with covariance $\boldsymbol{P}^i_{\mathcal{N}^{i,+}_{k-1}}$.

At measurement time k, for the ith particle ($i=1,2,\ldots,N$), let $t+1\to t$ and predict the state arriving time sample τ^i_t with parameters $\tau_{\min,t}$, α_t,

and β_t. To ensure a complete neighborhood at time k, repeat the above procedure until $\tau_t^i \geq k$. Let $\mathcal{N}_k^{i,-} = \mathcal{N}_{k-1}^{i,+}$ and $\mathcal{N}_k^{i,+} = t$, a complete neighborhood $\mathcal{N}_k^i$ at time k is established. Draw the acceleration sample $\boldsymbol{a}_t^i$ from $N(0, \boldsymbol{Q}_t)$. Now we can obtain the kinematic sample $\boldsymbol{\eta}_t^i$. Calculate the sigma point set using the unscented transformation (UT) (Julier *et al.*, 2000)

$$\boldsymbol{\mathcal{X}}^i_{\mathcal{N}_{k-1}^{i,+}} = \left[\begin{array}{cc} \bar{\boldsymbol{\eta}}^i_{\mathcal{N}_{k-1}^{i,+}} & \bar{\boldsymbol{\eta}}^i_{\mathcal{N}_{k-1}^{i,+}} \pm \sqrt{(n+\lambda)\boldsymbol{P}^i_{\mathcal{N}_{k-1}^{i,+}}} \end{array} \right], \tag{16}$$

where n is the state dimension, λ the UT parameter satisfying $n + \lambda > 0$. Predict the state sigma point set $\boldsymbol{\mathcal{X}}^i_{\mathcal{N}_k^{i,+}|\mathcal{N}_{k-1}^{i,+}}$ from Eqs. (4) and (5) with τ_t^i and $\boldsymbol{a}_t^i$. Estimate the mean and covariance of the state prediction:

$$\bar{\boldsymbol{\eta}}^i_{\mathcal{N}_k^{i,+}|\mathcal{N}_{k-1}^{i,+}} = \sum_{j=0}^{2n} W_j \boldsymbol{\mathcal{X}}^i_{j,\mathcal{N}_k^{i,+}|\mathcal{N}_{k-1}^{i,+}}, \tag{17}$$

$$\begin{aligned} \boldsymbol{P}^i_{\mathcal{N}_k^{i,+}|\mathcal{N}_{k-1}^{i,+}} =& \sum_{j=0}^{2n} W_j \left[\boldsymbol{\mathcal{X}}^i_{j,\mathcal{N}_k^{i,+}|\mathcal{N}_{k-1}^{i,+}} - \bar{\boldsymbol{\eta}}^i_{\mathcal{N}_k^{i,+}|\mathcal{N}_{k-1}^{i,+}} \right] \\ & \cdot \left[\boldsymbol{\mathcal{X}}^i_{j,\mathcal{N}_k^{i,+}|\mathcal{N}_{k-1}^{i,+}} - \bar{\boldsymbol{\eta}}^i_{\mathcal{N}_k^{i,+}|\mathcal{N}_{k-1}^{i,+}} \right]^{\mathrm{T}}, \end{aligned} \tag{18}$$

where $W_0 = \lambda/(n+\lambda)$ and $W_j = 1/[2(n+\lambda)]$ $(j \neq 0)$ are the sigma point weights (Julier *et al.*, 2000). Draw the measurement noise sample $\boldsymbol{v}_k^i$ from Eq. (7), and predict the measurement sigma point set $\boldsymbol{\mathcal{Z}}^i_{k|\mathcal{N}_{k-1}^{i,+}}$ with $\boldsymbol{v}_k^i$. Calculate the mean and covariance of measurement prediction:

$$\bar{\boldsymbol{z}}^i_{k|\mathcal{N}_{k-1}^{i,+}} = \sum_{j=0}^{2n} W_j \boldsymbol{\mathcal{Z}}^i_{j,k|\mathcal{N}_{k-1}^{i,+}}, \tag{19}$$

$$\begin{aligned} \boldsymbol{P}^i_{\boldsymbol{zz},k|\mathcal{N}_{k-1}^{i,+}} =& \sum_{j=0}^{2n} W_j \left[\boldsymbol{\mathcal{Z}}^i_{j,k|\mathcal{N}_{k-1}^{i,+}} - \bar{\boldsymbol{z}}^i_{k|\mathcal{N}_{k-1}^{i,+}} \right] \\ & \cdot \left[\boldsymbol{\mathcal{Z}}^i_{j,k|\mathcal{N}_{k-1}^{i,+}} - \bar{\boldsymbol{z}}^i_{k|\mathcal{N}_{k-1}^{i,+}} \right]^{\mathrm{T}}. \end{aligned} \tag{20}$$

Calculate the cross-covariance and Kalman gain:

$$\begin{aligned} \boldsymbol{P}^i_{\boldsymbol{\eta z},\mathcal{N}_k^{i,+}|\mathcal{N}_{k-1}^{i,+}} =& \sum_{j=0}^{2n} W_j \left[\boldsymbol{\mathcal{X}}^i_{j,\mathcal{N}_k^{i,+}|\mathcal{N}_{k-1}^{i,+}} - \bar{\boldsymbol{\eta}}^i_{\mathcal{N}_k^{i,+}|\mathcal{N}_{k-1}^{i,+}} \right] \\ & \cdot \left[\boldsymbol{\mathcal{Z}}^i_{j,k|\mathcal{N}_{k-1}^{i,+}} - \bar{\boldsymbol{z}}^i_{k|\mathcal{N}_{k-1}^{i,+}} \right]^{\mathrm{T}}, \end{aligned} \tag{21}$$

$$\boldsymbol{K}^i_{\mathcal{N}_k^{i,+}} = \boldsymbol{P}^i_{\boldsymbol{\eta z},\mathcal{N}_k^{i,+}|\mathcal{N}_{k-1}^{i,+}} \left[\boldsymbol{P}^i_{\boldsymbol{zz},k|\mathcal{N}_{k-1}^{i,+}} \right]^{-1}. \tag{22}$$

Update the mean and covariance:

$$\bar{\boldsymbol{\eta}}^i_{\mathcal{N}_k^{i,+}} = \bar{\boldsymbol{\eta}}^i_{\mathcal{N}_k^{i,+}|\mathcal{N}_{k-1}^{i,+}} + \boldsymbol{K}^i_{\mathcal{N}_k^{i,+}} \left(\boldsymbol{z}_k - \bar{\boldsymbol{z}}^i_{k|\mathcal{N}_{k-1}^{i,+}} \right), \tag{23}$$

$$\boldsymbol{P}^i_{\mathcal{N}_k^{i,+}} = \boldsymbol{P}^i_{\mathcal{N}_k^{i,+}|\mathcal{N}_{k-1}^{i,+}} - \boldsymbol{K}^i_{\mathcal{N}_k^{i,+}} \boldsymbol{P}^i_{\boldsymbol{zz},k|\mathcal{N}_{k-1}^{i,+}} \left(\boldsymbol{K}^i_{\mathcal{N}_k^{i,+}} \right)^{\mathrm{T}}. \tag{24}$$

Then draw particles from the following proposal pdf:

$$\breve{\boldsymbol{\eta}}^i_{\mathcal{N}_k^{i,+}} = \breve{\boldsymbol{\eta}}^i_t \sim q(\boldsymbol{\eta}^i_{\mathcal{N}_k^+}|\boldsymbol{\eta}^i_{\mathcal{N}_{k-1}^+}, \boldsymbol{z}_{0:k}) = N(\bar{\boldsymbol{\eta}}^i_{\mathcal{N}_k^{i,+}}, \boldsymbol{P}^i_{\mathcal{N}_k^{i,+}}). \tag{25}$$

Calculate the interpolation function with the state neighborhood:

$$\hat{\boldsymbol{\eta}}^i_k = \frac{(k - \tau_{\mathcal{N}_k^{i,-}})\breve{\boldsymbol{\eta}}_{\mathcal{N}_k^{i,+}} + (\tau_{\mathcal{N}_k^{i,+}} - k)\boldsymbol{\eta}_{\mathcal{N}_k^{i,-}}}{\mathcal{N}_k^{i,+} - \mathcal{N}_k^{i,-}}. \tag{26}$$

The corresponding important weight can be evaluated with the interpolation function as follows:

$$\breve{w}^i_k = w^i_{k-1} \frac{p(\boldsymbol{z}_k|\hat{\boldsymbol{\eta}}^i_k) p(\breve{\boldsymbol{\eta}}^i_{\mathcal{N}_k^{i,+}}|\boldsymbol{\eta}^i_{\mathcal{N}_{k-1}^+})}{q(\breve{\boldsymbol{\eta}}^i_{\mathcal{N}_k^{i,+}}|\boldsymbol{\eta}^i_{\mathcal{N}_{k-1}^+}, \boldsymbol{z}_{0:k})}. \tag{27}$$

Normalize the important weight and obtain w_k^i with $\breve{w}_k^i$.

3.4 Output and resampling

Usually, we are interested in the target state at the measurement sampling time. Hence, the output can be obtained by estimating the interpolation kinematic vector and its covariance at time k:

$$\hat{\boldsymbol{\eta}}_k = \sum_{i=1}^{N} w_k^i \hat{\boldsymbol{\eta}}_k^i, \tag{28}$$

$$\boldsymbol{P}_k = \sum_{i=1}^{N} w_k^i [\hat{\boldsymbol{\eta}}_k - \hat{\boldsymbol{\eta}}_k^i][\hat{\boldsymbol{\eta}}_k - \hat{\boldsymbol{\eta}}_k^i]^{\mathrm{T}}. \tag{29}$$

Then, one can predict the measurement $\hat{\boldsymbol{z}}_{k+1|k}$ and its covariance $\boldsymbol{S}_{k+1|k}$ with $\hat{\boldsymbol{\eta}}_k$ and $\boldsymbol{P}_k$ (Bar-Shalom *et al.*, 2001), which will be used in the next maneuver detection. Resample N new particles $\{\boldsymbol{\eta}^i_{\mathcal{N}_k^{i,+}}, \boldsymbol{P}^i_{\mathcal{N}_k^{i,+}}\}$ from $\{\breve{\boldsymbol{\eta}}^i_{\mathcal{N}_k^{i,+}}, \boldsymbol{P}^i_{\mathcal{N}_k^{i,+}}\}$ with the important weight w_k^i if necessary (Li *et al.*, 2015). Combine $\boldsymbol{\eta}^i_{\mathcal{N}_k^{i,+}}$ with $\tau_{\mathcal{N}_k^{i,+}}$ and $\boldsymbol{a}_{\mathcal{N}_k^{i,+}}$, and finally we obtain the weighted particles at time k, $\{\boldsymbol{X}^i_{\mathcal{N}_k^{i,+}}, w_k^i\}_{i=1}^N$.

In this section, the MVRPF algorithm is presented in detail. The proposed method is based on the Cartesian-coordinate model and can adjust

adaptively parameters using a maneuver-detection strategy. The state point distribution and the particle distribution are optimized without additional computational and storage burden. In the presence of small measurement errors, the UPF is adopted to yield the proposal pdf and hence can improve the estimation performance.

4 Simulation

The MVRPF method is implemented to track a maneuvering target in 2D space. To illustrate its performance, the proposed method is compared with the following methods: (1) the VRPF in the intrinsic coordinates, denoted by VRPF-I; (2) the VRPF in the Cartesian coordinates, denoted by VRPF-C; (3) the maneuver-detection based VRPF in the Cartesian coordinates, denoted by MD-VRPF.

The scenario parameters are given as follows. The initial target state is $\boldsymbol{X}_0 = [40\text{ m }2\text{ m/s }60\text{ m }2\text{ m/s}]^{\mathrm{T}}$. During the first 20 s, the target makes a nearly constant velocity motion with process noise standard derivation $\sigma_v = 0.01\text{ m/s}^2$. From $k = 21$ s to $k = 30$ s, it makes a constant turning motion with angle velocity $\omega_1 = -0.1164$ rad/s. Then it continues with a nearly constant velocity motion with $\sigma_v = 0.01\text{ m/s}^2$ for 20 s. From $k = 50$ s to $k = 55$ s, it makes another constant turning motion with angle velocity $\omega_2 = 0.6283$ rad/s. Then it makes a nearly constant velocity motion with $\sigma_v = 0.01\text{ m/s}^2$ until $k = 70$ s. The true target trajectory is shown in Fig. 2. The sensor is located at the origin and can obtain the target's range and bearing information with the scan interval of 1 s. The measurement functions are given as follows:

$$r_k = \sqrt{\xi_{x,k}^2 + \xi_{y,k}^2} + w_{r,k}, \tag{30}$$

$$\beta_k = \arctan\left(\xi_{x,k}/\xi_{y,k}\right) + w_{\beta,k}, \tag{31}$$

where measurement noise satisfies $w_{r,k} \sim N(0, \sigma_r^2)$, $\sigma_r = 1$ m, and $w_{\beta,k} \sim N(0, \sigma_\beta^2)$, $\sigma_\beta = 0.01$ rad.

The number of particles is 1000 and 100 Monte Carlo runs are tested. For the VRPF-I and VRPF-C methods, the shifted gamma distribution parameters are designed as $\tau_{\min} = 0.5, \alpha = 2$, and $\beta = 0.5$. Other parameters in each algorithm are given as follows: (1) VRPF-I (dimensionless)—the target mass is $m = 1$, the tangential force satisfies $T_P \sim N(0, 0.7^2)$, and the normal force follows $T_N \sim N(0, 0.5^2)$. (2) VRPF-C—the acceleration in each dimension satisfies $a \sim N(0, 0.5^2)$. (3) MD-VRPF and MVRPF—parameters in the non-maneuvering case are designed as $\tau_{\min}^0 = 0.5, \alpha^0 = 2$, $\beta^0 = 0.5$, and $Q^0 = 0.5^2$; parameters in the maneuvering case are given as $\tau_{\min}^1 = 0.3, \alpha^1 = 2$, $\beta^1 = 0.4$, and $Q^1 = 1^2$. The sliding window width is $l = 1$ and the confidence level of the Chi-square test is 95%. The UT parameter in MVRPF is $\lambda = -3$.

The estimated target trajectory and particle distribution with MVRPF in one run are illustrated in Fig. 3. We can observe that the target's maneuvering behaviors can be covered well by the particle's distribution scope. To illustrate the effect of maneuver detection on the distribution of state points, Figs. 4 and 5 show the trajectories of a single particle with VRPF and MVRPF in one run, respectively. It is shown that, without maneuver detection, the number of state points in a given region is irregular. However, with maneuver detection, more state points are allocated in the maneuvering regions and

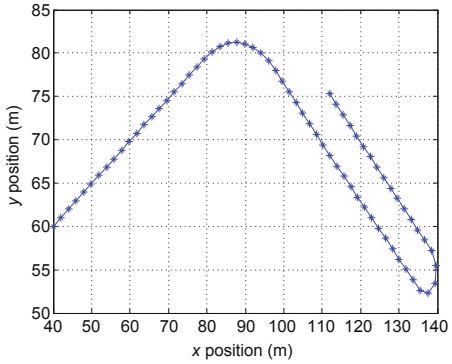

Fig. 2 True target trajectory

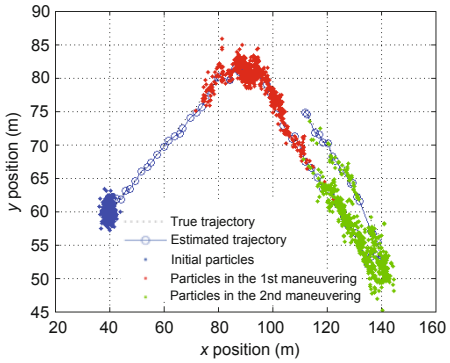

Fig. 3 Estimated target trajectory and particles

fewer in the smooth regions (Fig. 5). Thus, the distribution of state points is optimized with the proposed method. Note that in the fixed rate model framework, the number of state points of any particle is fixed and is equal to the number of scans, i.e., $k = 70$. However, in the variable rate model framework, the number of state points of a particle is variable and depends on the shifted gamma distribution. The average numbers of state points with different methods are listed in Tables 1 and 2.

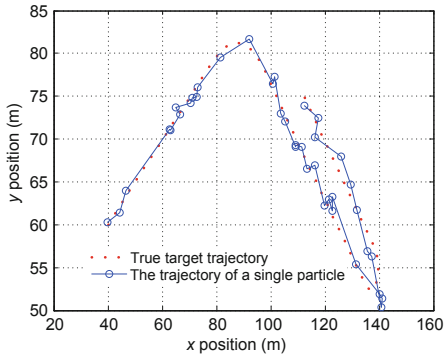

Fig. 4 The trajectory of a single particle with VRPF

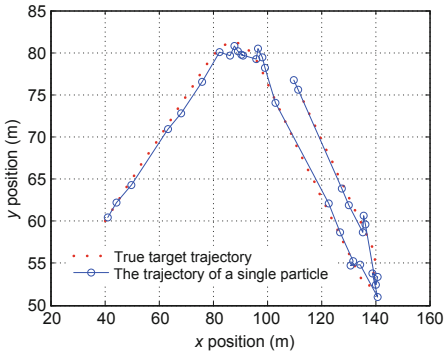

Fig. 5 The trajectory of a single particle with MVRPF

The estimation performance of different methods is evaluated by the following metrics: estimation precision, estimation credibility, computational complexity, and storage requirement. To compare the estimation precision, the root mean square errors (RMSE) of range estimate and velocity estimate are plotted in Figs. 6 and 7, respectively. It is shown that with these parameters aforementioned, four methods have comparable estimation precision in the non-maneuvering periods. In the maneuvering periods, MD-VRPF and MVRPF perform better than the others, and the proposed method achieves the best accuracy, especially in the second maneuvering period. The performance improvement of the proposed method benefits from both parameter adjustment and the improved proposal pdf. To illustrate the estimation credibility, Fig. 8 compares the average normalized estimation error squared (ANEES) curves (Li *et al.*, 2001) with an acceptance probability of 95%. Compared with the ANEES points with VRPF-I, more ANEES points lie

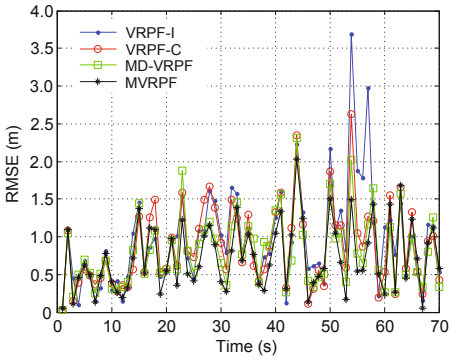

Fig. 6 Range RMSE curves of different methods under the first group of parameters

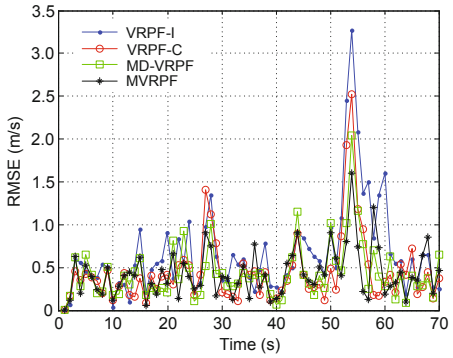

Fig. 7 Velocity RMSE curves of different methods under the first group of parameters

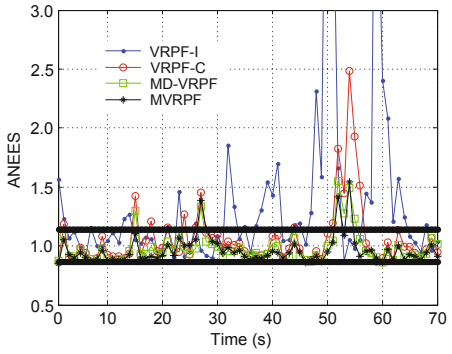

Fig. 8 Average normalized estimation error squared (ANEES) curves of different methods under the first group of parameters

in the acceptance interval [0.865,1.142] (Farina *et al.*, 2002) with the Cartesian-coordinate based methods. Consequently, for the scenario considered here, the Cartesian-coordinate based methods are more credible.

Table 1 shows the average number of state points (ANSP), the average elapsed time (AET) in one run, the mean time of delay (MTD), and the average RMSE of range estimate (RMSEr) and of velocity estimate (RMSEv) from 100 Monte Carlo runs. The computational times are obtained on a PC with Intel Core i5 CPU running at 2.4 GHz. It is shown that the average number of state points with the proposed method is about 85% of the number of scans (70). It is also shown that the average RMSE of the proposed method is lower than others at the cost of an acceptable increase in computational time. This is mainly due to the UPF used in the proposed method. The effect of the UPF on the computation complexity is a double-edged sword. On the one hand, it increases the computational time due to the unscented transformation; on the other hand, it decreases the resampling time due to providing a better proposal pdf (van der Merwe *et al.*, 2000). In addition, there is about a 1.1-s delay for detecting the maneuver.

Table 1 Results of 100 Monte Carlo runs

Item	ANSP	AET (s)	MTD (s)	RMSEr (m)	RMSEv (m/s)
VRPF-I	52	4.35	–	0.91	0.55
VRPF-C	53	4.43	–	0.87	0.44
MD-VRPF	59	5.42	1.12	0.81	0.40
MVRPF	60	6.86	1.14	0.74	0.37

ANSP: average number of state points; AET: average elapsed time; MTD: mean time of delay; RMSEr: average RMSE of range estimate; RMSEv: average RMSE of velocity estimate

To further improve the estimation precision, the second group of parameters are used in the non-maneuvering periods for MD-VRPF and MVRPF: $\tau_{\min}^0 = 0.7, \alpha^0 = 2$, $\beta^0 = 0.7$, and $Q^0 = 0.2^2$. The corresponding RMSE and ANEES curves are shown in Figs. 9–11, respectively. It is shown that the estimation accuracies of MD-VRPF and MVRPF in the non-maneuvering periods are improved by more appropriate parameters. Unfortunately, these parameters lead to filter divergence when applied in VRPF-I and VRPF-C, especially in the high maneuvering periods. In fact, for a single-model filter without a maneuvering detection strategy, the choice of parameters is a trade-off between the estimation performance during maneuvering periods and that during non-maneuvering periods (Bar-Shalom and Li, 1995). In other words, the proposed method allows a lower process noise level in the non-maneuvering periods.

Table 2 compares the performance metrics with the second group of parameters. It is shown that

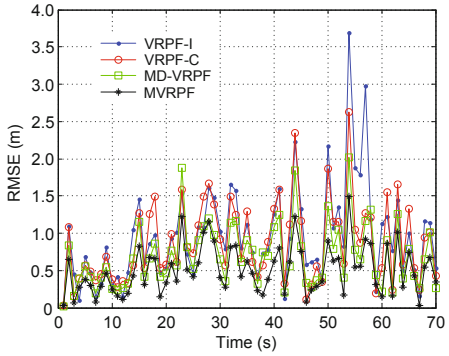

Fig. 9 Range RMSE curves of different methods under the second group of parameters

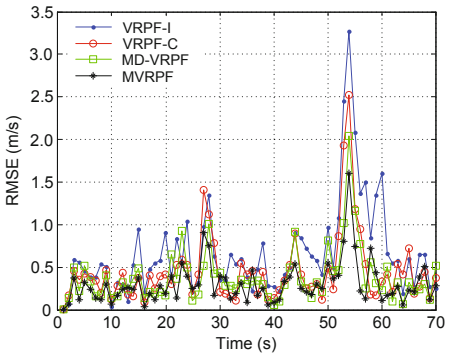

Fig. 10 Velocity RMSE curves of different methods under the second group of parameters

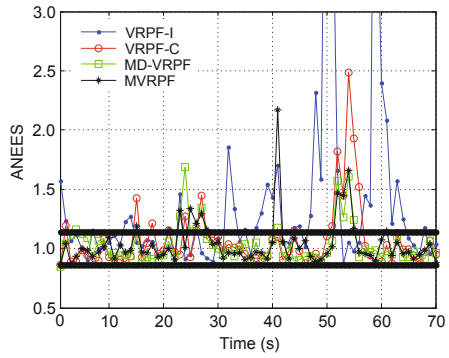

Fig. 11 Average normalized estimation error squared (ANEES) curves of different methods under the second group of parameters

with the second group of parameters, the ANSP with the proposed method reduces to 66% of the number of scans (70) and is fewer than that without maneuver detection. For the same target trajectory, fewer state points means a reduction in storage requirement and hence alleviates the communication load. It is very important for characterizing a trajectory with prolonged smooth regions and infrequent maneuvering regions. It is also shown that the average RMSE of the proposed method is lower than others. In addition, the AET decreases because fewer state points are needed to predict and update in the non-maneuvering periods.

Table 2 Results of 100 Monte Carlo runs with the second group of parameters

Item	ANSP	AET (s)	MTD (s)	RMSEr (m)	RMSEv (m/s)
VRPF-I	52	4.35	–	0.91	0.55
VRPF-C	53	4.43	–	0.87	0.44
MD-VRPF	46	4.57	1.12	0.73	0.34
MVRPF	46	5.54	1.14	0.53	0.30

ANSP: average number of state points; AET: average elapsed time; MTD: mean time of delay; RMSEr: average RMSE of range estimate; RMSEv: average RMSE of velocity estimate

5 Conclusions

In this paper, an MVRPF algorithm is proposed to address the problem of tracking a maneuvering target with prolonged non-maneuvering motions and abrupt maneuvering motions. A Cartesian-coordinate based variable rate model is presented, which is more convenient than the intrinsic-coordinate based model. Based on this model, a maneuver detection strategy and a parameter adjustment method are proposed to reduce the storage requirement and improve the estimation accuracy. In addition, a UPF is embedded in the proposed method to improve the tracking performance, in the presence of sharp likelihood. Future work will focus on multiple maneuvering targets tracking in heavy clutter using the proposed method.

References

Bar-Shalom, Y., Li, X.R., 1995. Multitarget-Multisensor Tracking: Principles and Techniques. Yaakov Bar-Shalom.

Bar-Shalom, Y., Li, X.R., Kirubarajan, T., 2001. Estimation with Applications to Tracking and Navigation. Johh Wiley & Sons, New York, USA.

Bunch, P., Godsill, S., 2013. Particle smoothing algorithms for variable rate models. *IEEE Trans. Signal Process.*, **61**(7):1663-1675. [doi:10.1049/iet-cta.2013.0472]

Farina, A., Ristic, B., Benvenuti, D., 2002. Tracking a ballistic target: comparison of several nonlinear filters. *IEEE Trans. Aerosp. Electron. Syst.*, **38**(3):854-867. [doi:10.1109/TAES.2002.1039404]

Godsill, S.J., Vermaak, J., Ng, W., *et al.*, 2007. Models and algorithms for tracking of maneuvering objects using variable rate particle filters. *Proc. IEEE*, **95**(5):925-952. [doi:10.1109/JPROC.2007.894708]

Julier, S., Uhlmann, J., Durrant-Whyte, H.F., 2000. A new method for the nonlinear transformation of means and covariances in filters and estimators. *IEEE Trans. Autom. Contr.*, **45**(3):477-482. [doi:10.1109/9.847726]

Li, T.C., Bolic, M., Djuric, P.M., 2015. Resampling methods for particle filtering: classification, implementation, and strategies. *IEEE Signal Process. Mag.*, **32**(3):70-86. [doi:10.1109/MSP.2014.2330626]

Li, X.R., Jilkov, V.P., 2003. Survey of maneuvering target tracking. Part I: dynamic models. *IEEE Trans. Aerosp. Electron. Syst.*, **39**(4):1333-1364. [doi:10.1109/TAES.2003.1261132]

Li, X.R., Jilkov, V.P., 2010. Survey of maneuvering target tracking. Part II: motion models of ballistic and space targets. *IEEE Trans. Aerosp. Electron. Syst.*, **46**(1):96-119. [doi:10.1109/TAES.2010.5417150]

Li, X.R., Zhao, Z.L., Jilkov, V.P., 2001. Practical measures and test for credibility of an estimator. Proc. Workshop on Estimation, Tracking, and Fusion: a Tribute to Yaakov Bar-Shalom, p.481-495.

Nemeth, C., Fearnhead, P., Mihaylova, L., 2014. Sequential Monte Carlo methods for state and parameter estimation in abruptly changing environments. *IEEE Trans. Signal Process.*, **62**(5):1245-1255. [doi:10.1109/TSP.2013.2296278]

Ru, J.F., Jilkov, V.P., Li, X.R., *et al.*, 2009. Detection of target maneuver onset. *IEEE Trans. Aerosp. Electron. Syst.*, **45**(2):536-554. [doi:10.1109/TAES.2009.5089540]

Schoenecker, S., Willett, P., Bar-Shalom, Y., 2013. The ML-PMHT multistatic tracker for sharply maneuvering targets. *IEEE Trans. Aerosp. Electron. Syst.*, **49**(4):2235-2249. [doi:10.1109/TAES.2013.6621813]

Ulker, Y., Gunsel, B., 2012. Multiple model target tracking with variable rate particle filters. *Dig. Signal Process.*, **22**(3):417-429. [doi:10.1016/j.dsp.2012.01.003]

van der Merwe, R., Doucet, A., de Freitas, N., *et al.*, 2000. The unscented particle filter. *NIPS*, p.584-590.

Whiteley, N., Johansen, A.M., Godsill, S., 2011. Monte Carlo filtering of piecewise deterministic processes. *J. Comput. Graph. Stat.*, **20**(1):119-139. [doi:10.1198/jcgs.2009.08052]

Yang, W., Wang, Z.X., Fu, Y.W., *et al.*, 2015. Joint detection, tracking and classification of a manoeuvring target in the finite set statistics framework. *IET Signal Process.*, **9**(1):10-20. [doi:10.1049/iet-spr.2013.0363]

Zhang, W., Zuo, J.Y., Guo, Q., *et al.*, 2015. Multisensor information fusion scheme for particle filter. *Electron. Lett.*, **51**(6):486-488. [doi:10.1049/el.2014.3051]

Zhang, Y.J., Geng, Z., 2013. Detection of target maneuver from bearings-only measurements. *IEEE Trans. Aerosp. Electron. Syst.*, **49**(3):2028-2034. [doi:10.1109/TAES.2013.6558036]

Zuo, J.Y., Jia, Y.N., Zhang, Y.Z., *et al.*, 2013. Adaptive iterated particle filter. *Electron. Lett.*, **49**(12):742-744. [doi:10.1049/el.2012.4506]